EINDHOVEN UNIVERSITY OF TECHNOLOGY

Identification of the Origin of Ultralow Dark Currents in Organic Photodiodes

Citation for published version (APA):
Ma, X., Bin, H., van Gorkom, B. T., van der Pol, T. P. A., Dyson, M. J., Weijtens, C. H. L., Fattori, M., Meskers, S. C. J., van Breemen, A. J. J. M., Tordera, D., Janssen, R. A. J., & Gelinck, G. H. (2023). Identification of the Origin of Ultralow Dark Currents in Organic Photodiodes. *Advanced Materials*, *35*(8), Article 2209598. https://doi.org/10.1002/adma.202209598

DOI:
10.1002/adma.202209598

Document status and date:
Published: 23/02/2023

Document Version:
Publisher's PDF, also known as Version of Record (includes final page, issue and volume numbers)

Please check the document version of this publication:

• A submitted manuscript is the version of the article upon submission and before peer-review. There can be important differences between the submitted version and the official published version of record. People interested in the research are advised to contact the author for the final version of the publication, or visit the DOI to the publisher's website.
• The final author version and the galley proof are versions of the publication after peer review.
• The final published version features the final layout of the paper including the volume, issue and page numbers.

Link to publication

General rights
Copyright and moral rights for the publications made accessible in the public portal are retained by the authors and/or other copyright owners and it is a condition of accessing publications that users recognise and abide by the legal requirements associated with these rights.

• Users may download and print one copy of any publication from the public portal for the purpose of private study or research.
• You may not further distribute the material or use it for any profit-making activity or commercial gain
• You may freely distribute the URL identifying the publication in the public portal.

If the publication is distributed under the terms of Article 25fa of the Dutch Copyright Act, indicated by the "Taverne" license above, please follow below link for the End User Agreement:

www.tue.nl/taverne

Take down policy
If you believe that this document breaches copyright please contact us at:

openaccess@tue.nl

providing details and we will investigate your claim.

Download date: 04. Oct. 2023

Check for updates

ADVANCED MATERIALS
www.advmat.de

Identification of the Origin of Ultralow Dark Currents in Organic Photodiodes

Xiao Ma, Haijun Bin, Bas T. van Gorkom, Tom P. A. van der Pol, Matthew J. Dyson, Christ H. L. Weijtens, Marco Fattori, Stefan C. J. Meskers, Albert J. J. M. van Breemen, Daniel Tordera, René A. J. Janssen, and Gerwin H. Gelinck*

Organic bulk heterojunction photodiodes (OPDs) attract attention for sensing and imaging. Their detectivity is typically limited by a substantial reverse bias dark current density (J_d). Recently, using thermal admittance or spectral photocurrent measurements, J_d has been attributed to thermal charge generation mediated by mid-gap states. Here, the temperature dependence of J_d in state-of-the-art OPDs is reported with J_d down to 10^{-9} mA cm^{-2} at –0.5 V bias. For a variety of donor-acceptor bulk-heterojunction blends it is found that the thermal activation energy of J_d is lower than the effective bandgap of the blends, by ca. 0.3 to 0.5 eV, but higher than expected for mid-gap states. Ultra-sensitive sub-bandgap photocurrent spectroscopy reveals that the minimum photon energy for optical charge generation in OPDs correlates with the dark current thermal activation energy. The dark current in OPDs is attributed to thermal charge generation at the donor-acceptor interface mediated by intra-gap states near the band edges.

X. Ma, H. Bin, B. T. van Gorkom, T. P. A. van der Pol, M. J. Dyson, C. H. L. Weijtens, S. C. J. Meskers, R. A. J. Janssen, G. H. Gelinck
Molecular Materials and Nanosystems and Institute for Complex Molecular Systems
Eindhoven University of Technology
P.O. Box 513, Eindhoven 5600 MB, The Netherlands
E-mail: r.a.j.janssen@tue.nl

M. Fattori
Integrated Circuits
Department of Electrical Engineering
Eindhoven University of Technology
P.O. Box 513, Eindhoven 5600 MB, The Netherlands

A. J. J. M. van Breemen, D. Tordera, G. H. Gelinck
TNO/Holst Centre
High Tech Campus 31
Eindhoven 5656 AE, The Netherlands

D. Tordera
Instituto de Ciencia Molecular (ICMol)
Universidad de Valencia
C/ Catedrático J. Beltrán 2, Paterna 46980, Spain

R. A. J. Janssen
Dutch Institute for Fundamental Energy Research
De Zaale 20, Eindhoven 5612 AJ, The Netherlands

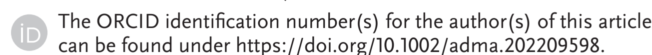
The ORCID identification number(s) for the author(s) of this article can be found under https://doi.org/10.1002/adma.202209598.

© 2022 The Authors. Advanced Materials published by Wiley-VCH GmbH. This is an open access article under the terms of the Creative Commons Attribution License, which permits use, distribution and reproduction in any medium, provided the original work is properly cited.

DOI: 10.1002/adma.202209598

1. Introduction

With ever-growing demands for light sensing and imaging in industry and consumer electronics, organic photodiodes (OPDs) attract extensive attention for emerging applications such as wearable monitoring,[1,2] biomedical imaging,[3–5] surveillance systems, and machine vision.[6] Organic semiconductors present high tunability in optoelectronic properties[7] and provide a promising pathway to achieve flexible and lightweight devices.[8] Significant progress in developing donor-acceptor (D–A) bulk-heterojunction (BHJ) OPDs has led to near 100% external quantum efficiency (EQE),[9] and > 100% EQE has been reported for photomultiplication type OPDs.[10–14] Despite these high EQE values the specific detectivity (D^*) of OPDs is still rather low and typically limited by the high noise current spectral density (i_n) that primarily stems from the reverse bias dark current density (J_d). Understanding the factors that determine J_d is an important prerequisite to further reduce J_d and thereby improve D^*.

Optimization of the device architecture has been proven to successfully suppress the overall reverse dark current in OPDs, e.g., by increasing active layer thickness,[15–17] adding charge blocking layers,[18–23] and improving energetic alignment of transport layers.[24,25] These measures mainly reduce leakage current from shunt paths or block injection current from non-ohmic contacts, but still cannot fully explain the relatively high J_d of OPDs compared to inorganic photodiodes with similar bandgaps. A more intrinsic mechanism of dark current generation is related to the presence of trap states in organic semiconductors. Shekhar et al. investigated the dark current for planar heterojunction OPDs by temperature-dependent J_d measurements and found that activation energies are too low to be related with effective bandgaps. According to the sub-gap EQE spectra, they considered deep tail states as one of the main sources of the J_d.[26] Kublitski et al.[27] and Zarrabi et al.[28] analyzed trap states in BHJ devices using thermal admittance and ultra-sensitive EQE measurements, respectively. Following a modified Shockley-Read-Hall (SRH) mechanism they concluded that mid-gap trap states in BHJs are responsible for the high reverse dark currents.[27,28]

© 2022 The Authors. Advanced Materials published by Wiley-VCH GmbH

15214095, 2023, 8, Downloaded from https://onlinelibrary.wiley.com/doi/10.1002/adma.202209598 by Technical University Eindhoven, Wiley Online Library on [03/03/2023]. See the Terms and Conditions (https://onlinelibrary.wiley.com/terms-and-conditions) on Wiley Online Library for rules of use; OA articles are governed by the applicable Creative Commons License

Where previous reports were based on BHJ devices with relatively high J_d, we present and investigate the temperature and bias dependence of J_d in state-of-the-art BHJ diodes with J_d as low as 10^{-9} mA cm^{-2} at –0.5 V bias, which enable to investigate the intrinsic origin of J_d. We find that J_d is thermally activated with an activation energy (E_a) that is much larger than expected for mid-gap states. Instead, we find a clear correlation of E_a with the low-energy onset of the photocurrent spectra (E_{onset}) and with the open-circuit voltage energy (qV_{OC}) of the devices under standard solar illumination. From the close correspondence of E_a, E_{onset}, and qV_{OC} we conclude that J_d in BHJ OPDs originates from thermal charge generation at the D–A interface involving sub-bandgap states close to the band edges of the donor and acceptor.

2. Results and Discussion

2.1. Thermally Activated Dark Current in BHJ Photodiodes

BHJ diodes were fabricated using six D–A combinations with effective bandgaps, ranging from 0.95 to 1.30 eV. The chemical structures and full names of the different donor polymers and acceptor molecules are provided in Figure S1 and Table S1 (Supporting Information). The energies of the highest occupied molecular orbital (HOMO) of the donors were determined by ultraviolet photoelectron spectroscopy (UPS) (Figure S2, Supporting Information). The energies of the lowest unoccupied molecular orbital (LUMO), determined by inverse photoemission spectroscopy (IPES), were taken from the literature[29,30] (Figure S3, Supporting Information). **Table 1** lists the resulting values for the effective bandgap (E_g^{eff}), taken as the energy difference between the LUMO of the acceptor and the HOMO of the donor. **Figure 1**a,b shows schematic cross sections of the complete photodiode stacks used in the dark current study. Unless denoted otherwise, the so-called standard configuration is used in which the photoactive BHJ layer is sandwiched between Mo/MoO_3 and LiF/Al (or *N*,*N*'-bis(*N*,*N*-dimethylpropan-1-amine oxide)perylene-3,4,9,10-tetracarboxylic diimide (PDINO)/Ag) top electrodes (Figure 1a). In the inverted stack (Figure 1b), indium tin oxide (ITO) covered with amorphous indium-gallium-zinc oxide (IGZO) was used as an electron-collecting electrode together with a thermally evaporated MoO_3/Ag hole-collecting top electrode. In both device configurations the metal (Al or Ag) top electrodes are thick, thus effectively shielding the photoactive layer from any spurious amounts of low-intensity ambient light. In both the standard and the inverted diode, an edge cover layer (ECL) consisting of an epoxy-based negative photoresist (SU-8) was used to cover the edges of the bottom electrode to minimize leakage currents.[8,31] The active area of the OPDs, as defined by the ECL, was 1 mm^2 and the BHJ thickness was kept constant at ca. 280 nm for all diodes by adjusting spin speed and/or the D–A concentration of the casting solvent. Further experimental details on materials and device fabrication are provided in the Supporting Information.

The current density – voltage (J–V) characteristics at room temperature (295 K) of the six BHJ diodes are shown in Figure 1c. The solid lines represent current densities measured in forward and backward voltage scans, and the symbols represent J_d values measured at constant applied voltages. Small differences between forward and backward voltage scans occur for BHJ diodes with very low current densities. These are attributed to capacitive charging effects. Such displacement currents are manifest themselves by non-zero J_d at 0 V. The constant-voltage method eliminates transient effects due to displacement and charging, and is therefore considered the more accurate method to measure low current levels.[31,32] When mentioning J_d values we will always refer to measurements done at constant bias (shown as symbols) for the reasons given above. All diodes show a nearly ideal diode behavior under forward bias. The dark current density at –0.5 V ranges from 10^{-5} to 10^{-9} mA cm^{-2}, decreasing with increasing E_g^{eff}, as reported previously.[31,33] As expected for diodes with such low J_d values, their i_n values are also very low, ranging from 3×10^{-14} to 7×10^{-15} A Hz$^{-1/2}$ for a bias voltage of –0.5 V and frequency of 1 Hz (Figure S4, Supporting Information). To our knowledge, for any given D–A combination, these diodes have J_d and i_n values on par or better than the corresponding D–A devices in the literature.[23,24,28,34–36] We attribute this to careful device optimization together with the use of an ECL and a relatively thick BHJ layer of 280 ± 10 nm. The ultralow J_d in these diodes provides a thus far unparalleled opportunity to investigate its intrinsic origin and explore possible mechanisms to further reduce the J_d in OPDs.

Figure 1d shows the J–V characteristics of the PDPP3T:PCBM BHJ diode measured at different temperatures. Similar results are shown for the five other BHJ diodes in Figure S5 (Supporting Information). Notably, the relative increase in dark current with increasing temperature is higher in reverse bias than

Table 1. Effective bandgap (E_g^{eff}), activation energy (E_a), open-circuit voltage energy (qV_{OC}), and E_{onset} for six D–A combinations. E_a is averaged over activation energies at different biases from –0.1 to –0.5 V and standard deviation is given. V_{OC} is measured under simulated solar illumination with an experimental error of ±0.01 V.

BHJ	E_g^{eff} [eV]	E_a [eV]	$E_g^{eff} - E_a$ [eV]	qV_{OC} [eV]	E_{onset} [eV]
PCDTBT:PCBM	1.30	0.86 ± 0.05	0.44 ± 0.05	0.81 ± 0.01	0.89
PTB7-Th:PCBM	1.20	0.76 ± 0.03	0.45 ± 0.03	0.80 ± 0.01	0.79
PM7:Y6	1.25	0.75 ± 0.03	0.32 ± 0.02	0.77 ± 0.01	0.76
PDPP3T:PCBM	1.05	0.73 ± 0.01	0.50 ± 0.02	0.68 ± 0.01	0.71
PTB7-Th:IEICO-4F	1.15	0.65 ± 0.02	0.41 ± 0.01	0.68 ± 0.01	0.66
PTB7-Th:Y6	0.95	0.54 ± 0.01	0.50 ± 0.03	0.55 ± 0.01	0.59

© 2022 The Authors. Advanced Materials published by Wiley-VCH GmbH

15214095, 2023, 8, Downloaded from https://onlinelibrary.wiley.com/doi/10.1002/adma.202209598 by Technical University Eindhoven, Wiley Online Library on [03/03/2023]. See the Terms and Conditions (https://onlinelibrary.wiley.com/terms-and-conditions) on Wiley Online Library for rules of use; OA articles are governed by the applicable Creative Commons License

15214095, 2023, 8, Downloaded from https://onlinelibrary.wiley.com/doi/10.1002/adma.202209598 by Technical University Eindhoven, Wiley Online Library on [03/03/2023]. See the Terms and Conditions (https://onlinelibrary.wiley.com/terms-and-conditions) on Wiley Online Library for rules of use; OA articles are governed by the applicable Creative Commons License

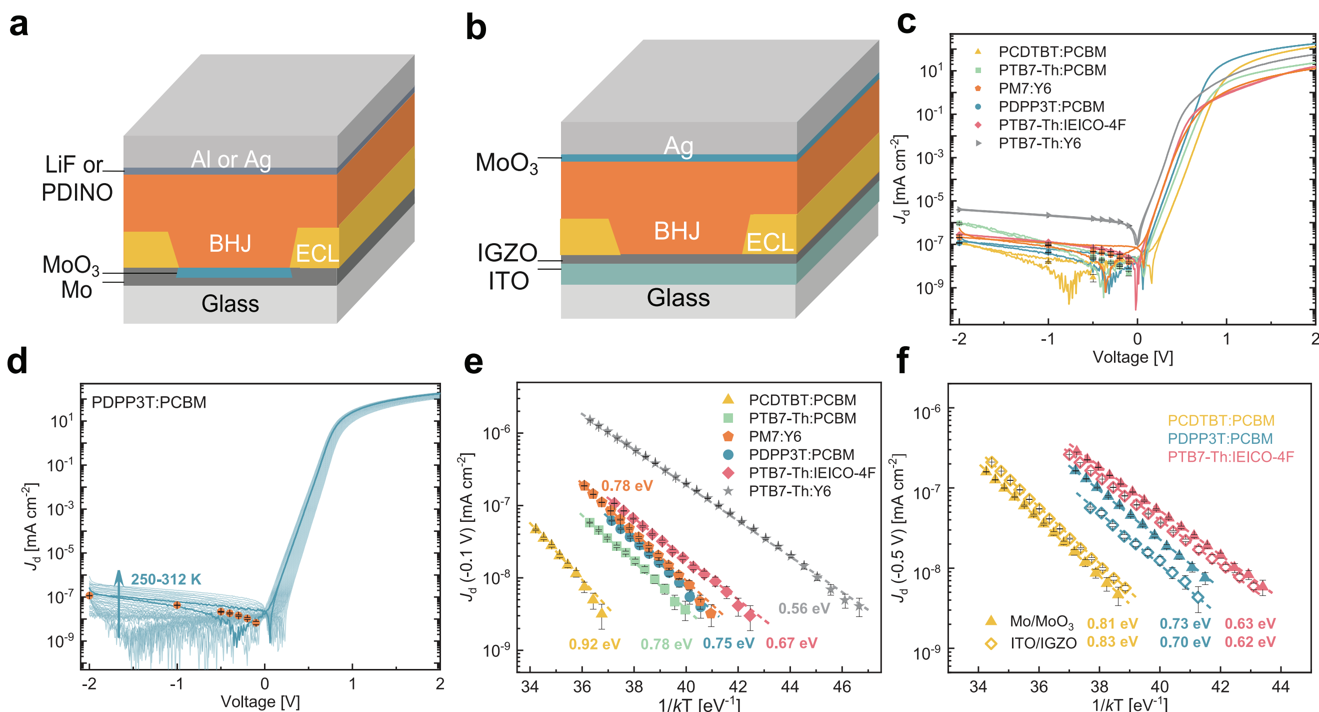

Figure 1. a,b) Schematic layout showing the device stack configurations: standard stack a) and inverted stack b). c) J–V characteristics of BHJ diodes for six D–A combinations in the standard stack configuration measured at room temperature. Lines represent forward and backward voltage scans. Symbols represent current density values obtained under constant voltage conditions and error bars on symbols are the standard deviation. d) J–V characteristics of PDPP3T:PCBM diodes in the standard stack configuration measured at different temperatures. The bold line denotes the J–V curve at room temperature. Symbols represent current density values obtained under constant voltage conditions at room temperature. e) Arrhenius plot of the temperature dependence of dark current density for six D–A BHJ diodes in the standard stack configuration. A voltage of −0.1 V was applied and error bars on symbols are the standard deviation. Lines are fits to the Arrhenius equation and the corresponding activation energies are shown next to the fits. f) Arrhenius plot of the temperature dependence of dark current density for three D–A BHJ diodes in standard (solid triangles) and inverted (empty diamonds) stack configurations. A voltage of −0.5 V was applied and error bars on symbols are the standard deviation.

in forward bias. In forward bias, the current is space-charge limited and the increase with temperature can be explained by a temperature-dependent mobility of injected charge carriers.[37] In reverse bias, the current originates from thermal charge generation and is determined by intra-gap states and the HOMO and LUMO energy levels. Figure 1e shows Arrhenius plots of J_d at −0.1 V for all diodes. In each case, the data can be accurately fitted to $J_d \propto \exp(-E_a/kT)$, with T the absolute temperature, k the Boltzmann constant, and a single exponent E_a. This indicates that the temperature dependence corresponds to a single thermal activation process (within the temperature range studied). The activation energy E_a (measured at −0.1 V bias) varies for the different D–A combinations from 0.56 to 0.92 eV (Figure 1e). As can be seen in Figure 1c,d (and Figure S5, Supporting Information), J_d shows a clear voltage dependence in the reverse-bias region. E_a also varies with the applied bias (Figure S6, Supporting Information). As an example, E_a decreases from 0.75 eV (at −0.1 V) to 0.58 eV (at −2.0 V) for the PDPP3T:PCBM blend. The largest reduction in E_a occurs, however, at high reverse bias, below −0.5 V. In contrast, E_a remains almost constant around 0.73 ± 0.01 eV between −0.1 and −0.5 V. This is an argument to rule out injection current as the main source of dark current between −0.1 and −0.5 V in these OPDs. This is typical for all BHJs. Using so-called Poole-Frenkel plots (see Figure S7 and Note S1, Supporting Information), we verify that in each case the J_d is close to voltage independent in the range from −0.1 to −0.5 V, and Table 1 lists the average E_a values measured in this voltage range.

We note that non-optimized devices, e.g., without ECL or thinner active layers, often showed J_d behavior that was non-Arrhenius like and less thermally activated than in optimized OPDs. We therefore, believe that a high activation energy of J_d, as found, is a sign of device quality.

For each D–A blend the activation energy E_a is distinctively smaller than its effective bandgap E_g^{eff} but significantly larger than $E_g^{\text{eff}}/2$, suggesting that J_d is unlikely related to mid-gap states. For example, the PCDTBT:PCBM blend has an effective bandgap of 1.30 eV and an activation energy of 0.86 eV (Table 1). The difference between E_a and E_g^{eff} for the six investigated BHJs ranges from ca. 0.3 to 0.5 eV (Table 1). The reason for this energy difference will be discussed later in more detail.

Three BHJs (PCDTBT:PCBM, PDPP3T:PCBM, and PTB7-Th:IEICO-4F) were also fabricated in the inverted device configuration (Figure 1b). The temperature dependence of J_d in the standard and inverted configurations are compared in Figure 1f. For the same BHJ layer, the differences between J_d values are less than a factor of 2 and the absolute differences between their E_as are within 0.03 eV. The negligible variation between the two stack configurations suggests that the thermal activation process of dark current in BHJ diodes is not affected

© 2022 The Authors. Advanced Materials published by Wiley-VCH GmbH

15214095, 2023, 8, Downloaded from https://onlinelibrary.wiley.com/doi/10.1002/adma.202209598 by Technical University Eindhoven, Wiley Online Library on [03/03/2023]. See the Terms and Conditions (https://onlinelibrary.wiley.com/terms-and-conditions) on Wiley Online Library for rules of use; OA articles are governed by the applicable Creative Commons License

by charge transport layers or contacts, and that the activation energy of J_d is solely determined by the BHJ.

2.2. Bulk Thermal Generation at the D–A Interface as the Origin of Dark Current

It is often argued that the reverse bias dark current originates from the injection current from contacts; thus, inserting charge blocking layers (CBL) between the contacts and active layer can increase the injection barrier and lower J_d.[18–23] Specifically, the deeper HOMO level of a hole blocking layer (HBL) increases the barrier for hole injection under reverse bias and, correspondingly, a shallower LUMO level of an electron blocking layer (EBL) increases the injection barrier for electrons. In an attempt to increase E_a and further reduce J_d, a C_{60} HBL (50 nm) was chosen and inserted between the active layer and LiF/Al cathode for three BHJs: PCDTBT:PCBM, PDPP3T:PCBM, and PTB7-Th:IEICO-4F. In **Figure 2**a, the Arrhenius plots of the temperature-dependent J_d recorded at –0.5 V show that the activation energies only change slightly for diodes with an additional C_{60} HBL. The absolute differences between the E_as are within 0.03 eV and the differences between the J_ds are less than a factor of 3, and within the device-to-device variation as shown in Figure S8 (Supporting Information). Considering the much deeper HOMO level of C_{60} (6.4 eV) compared to the HOMO of the three polymers (5.15, 4.90, and 5.05 eV), this indicates that a HBL with deeper HOMO level does not change the thermal activation of J_d making it unlikely that hole injection from cathode to HOMO of acceptor dominates the reverse J_d.

Polymer-only and bi-layer (polymer/C_{60}) diodes were made and compared with the BHJ diodes. The temperature dependence of J_d of PDPP3T-based diodes is shown in Figure 2b. The full current density – voltage characteristics are shown in Figure S9 (Supporting Information). At room temperature ($1/kT \approx 39$ eV^{-1}) an extremely low J_d (<10^{-9} mA cm^{-2} at –0.5 V bias) was achieved in the PDPP3T-only diode. This makes sense, given the relatively large E_g of PDPP3T (1.33 eV). After adding a C_{60} layer to form a bi-layer diode, the device shows a much higher J_d (more than one order of magnitude) than the PDPP3T-only device, and E_a reduces from 1.07 eV to 0.70 eV. This change in E_a is very close to the LUMO energy difference (0.38 eV) between PDPP3T (–3.60 eV) and C_{60} (–3.98 eV).[30] It strongly suggests that the lower activation barrier in the bi-layer device is caused by the deeper LUMO level of C_{60} and the charge carriers form at the D–A interface in the dark.

It is interesting to compare the PDPP3T/C_{60} bi-layer diode with the PDPP3T:PCBM BHJ diode. With E_a = 0.73 eV, the PDPP3T:PCBM BHJ has a similar thermal activation energy as the PDPP3T/C_{60} bilayer (0.70 eV). This may be expected because the LUMO energy of C_{60} of –3.98 eV is very close to that of PCBM (–3.85 eV).[30] Interestingly, the J_d of the bilayer diode is a factor of 10 lower than that of the BHJ (Figure 2b),

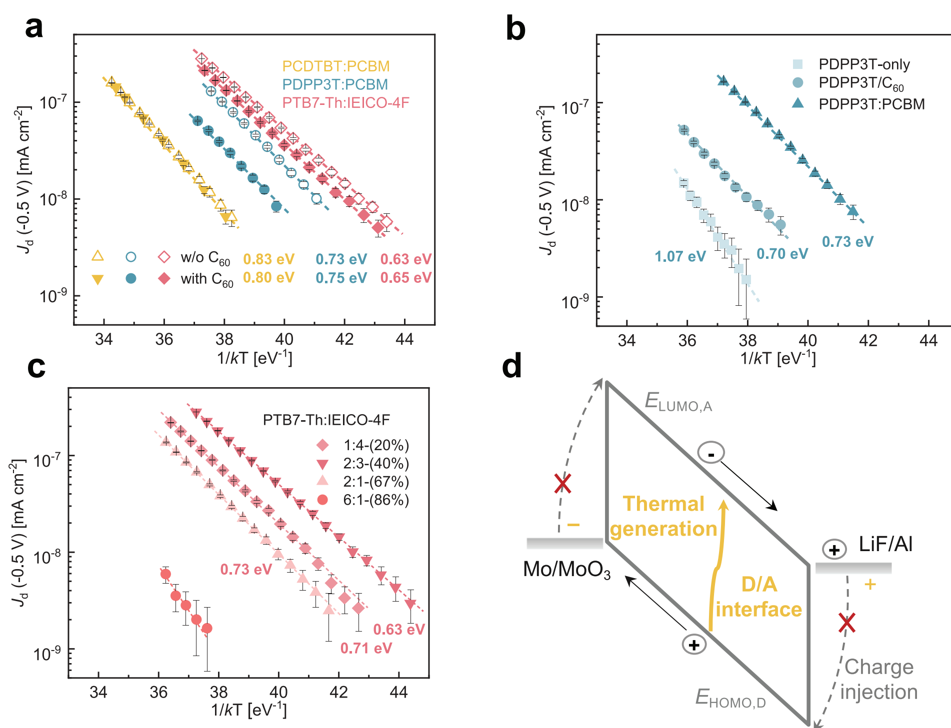

Figure 2. Bulk thermal generation at the D–A interface as the origin of dark current. Temperature dependence of J_d measured at –0.5 V for diodes with different active layers in standard stack configuration. Dotted lines denote Arrhenius-type fits and activation energies are shown next to fits. The error bars on symbols are the standard deviation of J_d. a) BHJs (PCDTBT:PCBM, PDPP3T:PCBM, and PTB7-Th:IEICO-4F) without and with C_{60} hole blocking layer. b) PDPP3T-only, PDPP3T/C_{60} bilayer and PDPP3T:PCBM BHJ. c) PTB7-Th:IEICO-4F BHJs with various D–A weight ratios (6:1, 2:1, 2:3, 1:4). d) Schematic diagram illustrating dark thermal charge generation current (yellow arrow) in the bulk and charge injection current from contacts (gray dashed arrow).

© 2022 The Authors. Advanced Materials published by Wiley-VCH GmbH

which we ascribe to the much smaller D–A interface area in the planar bilayer device compared to the BHJ.

An analogous trend is also observed between the PTB7-Th-only and PTB7-Th/C_{60} diodes in Figure S10 (Supporting Information). Due to the even larger E_g of PTB7-Th (1.65 eV), the PTB7-Th-only diode shows an extremely low J_d, reaching to the noise floor of the measurement setup (10^{-9} mA cm^{-2}) for the entire temperature region studied. After adding a C_{60} layer and forming the bi-layer diode, the J_d increases but is still close to the noise floor, and it is difficult to extract a clear E_a. However, the increase in J_d in PTB7-Th/C_{60} versus PTB7-Th-only diodes is visible, and consistent with that of PDPP3T series. Figure 2c shows the temperature dependence of J_d for PTB7-Th:IEICO-4F BHJs for different D–A ratios. The corresponding J–V curves at room temperature are shown in Figure S11 (Supporting Information). Going from a donor-rich blend to an acceptor-rich blend (i.e., decreasing the D:A weight ratio from 6:1, via 2:1 and 2:3, to 1:4), J_d first increases and then decreases. The highest J_d is found for a D–A weight ratio of 2:3, i.e., when the D–A interface area is expected to be largest. Collectively these results strongly suggests that at reverse bias dark thermal charge generation at the D–A interface is the primary cause of J_d as depicted in Figure 2d, rather than the injection of charges from the charge transport layers.

2.3. Relation Between the Open-Circuit Voltage and Activation Energy

Figure 3a compares E_a with E_g^{eff} and with the open-circuit voltage energy (qV_{OC}) of the corresponding BHJ solar cells measured under simulated AM1.5G illumination. There is an initially surprising correspondence between E_a and qV_{OC} for the six BHJs (Figure 3b). The energy difference between qV_{OC} and E_a is $< \pm$ 0.05 eV in all cases and the solid line represents $qV_{OC} = E_a$, i.e., a correlation with a slope of unity. The V_{OC} of a BHJ solar cell is directly related to the energy (E_{CT}) of the charge-transfer (CT) state at the D–A interface.[38] In turn, E_{CT} is strongly correlated to E_g^{eff}, as well as to being affected by the spatial separation of hole and electron in the CT state and the degree of polarization stabilization.[39] In BHJ solar cells, qV_{OC} is typically 0.5 to 0.6 eV below E_{CT} as a consequence of radiative and non-radiative recombination of holes and electrons generated under illumination.[40,41] The correlation between E_a and qV_{OC} can be understood by considering that qV_{OC} equals the splitting between the quasi-Fermi levels of the hole and electron distributions under illumination. Because of extensive non-radiative charge recombination in organic BHJs, these quasi-Fermi levels are located in the outer tails of the band edges. These outer tails of the band edges are also available for thermal charge generation and this can rationalize the empirical relationship between E_a and qV_{OC} (Figure 3b).[31,33] We note that in the current understanding of the origin of the V_{OC} of BHJ solar cells, mid-gap states are not involved.

2.4. Low-Energy Transitions in Sub-Bandgap EQE Spectra

Similar to Zarrabi et al.,[28] we employ ultra-sensitive photocurrent measurements to characterize the intra-gap states in more detail. **Figure 4**a shows the EQE spectra of semi-transparent devices for the six D–A combinations fabricated on ITO-covered glass substrates and employing an ITO back electrode (ITO/ZnO/BHJ/MoO_3/ITO), where ZnO and MoO_3 layers were used as electron and hole transport layers, respectively. The semi-transparent stack configuration minimizes the effects of light interference on the intensity of the sub-bandgap spectra that hampers extraction of reliable energetic information from peak positions.[28,42,43] A distinct low-energy band is seen below the exponential band edge of the BHJ for each D-A combination. These low-energy transitions in the EQE spectra demonstrate that photons with an energy less than the optical bandgap can produce a photocurrent and provide extractable charges. Because the photon energy is less than the bandgap this must involve intra-gap states. The low-energy onsets (E_{onset}) in these spectra represent the lowest-energy photo-excitations that generate photocurrent in the BHJ. While interference affects the optical electric field and thereby the shape of the EQE spectrum,[42] E_{onset} is mainly determined by material properties as found by comparing the BHJ photocurrent spectra in semi-transparent and non-transparent (ITO/PEDOT:PSS/BHJ/MoO_3/Ag) device configurations (Figure S13,

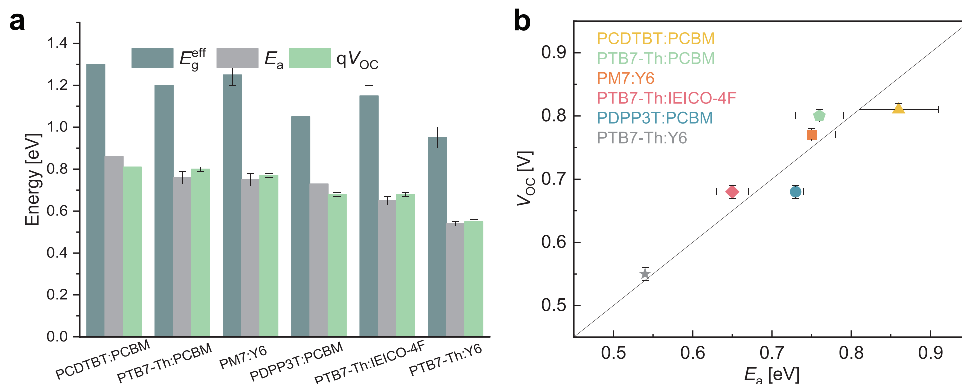

Figure 3. a) Comparison between effective bandgap of BHJ (E_g^{eff}), average activation energy (E_a), and open-circuit voltage energy (qV_{OC}). All values are from Table 1. V_{OC} is measured under simulated solar illumination with an experimental error of ±0.01 V and a device stack configuration of ITO/ZnO/BHJ/MoO_3/ITO is used. The J–V curves are shown in Figure S12 (Supporting Information). b) Open-circuit voltage plotted versus activation energy with the same error bars as in a). The gray line represents the relation of $qV_{OC} = E_a$.

© 2022 The Authors. Advanced Materials published by Wiley-VCH GmbH

15214095, 2023, 8, Downloaded from https://onlinelibrary.wiley.com/doi/10.1002/adma.202209598 by Technical University Eindhoven, Wiley Online Library on [03/03/2023]. See the Terms and Conditions (https://onlinelibrary.wiley.com/terms-and-conditions) on Wiley Online Library for rules of use; OA articles are governed by the applicable Creative Commons License

15214095, 2023, 8, Downloaded from https://onlinelibrary.wiley.com/doi/10.1002/adma.202209598 by Technical University Eindhoven, Wiley Online Library on [03/03/2023]. See the Terms and Conditions (https://onlinelibrary.wiley.com/terms-and-conditions) on Wiley Online Library for rules of use; OA articles are governed by the applicable Creative Commons License

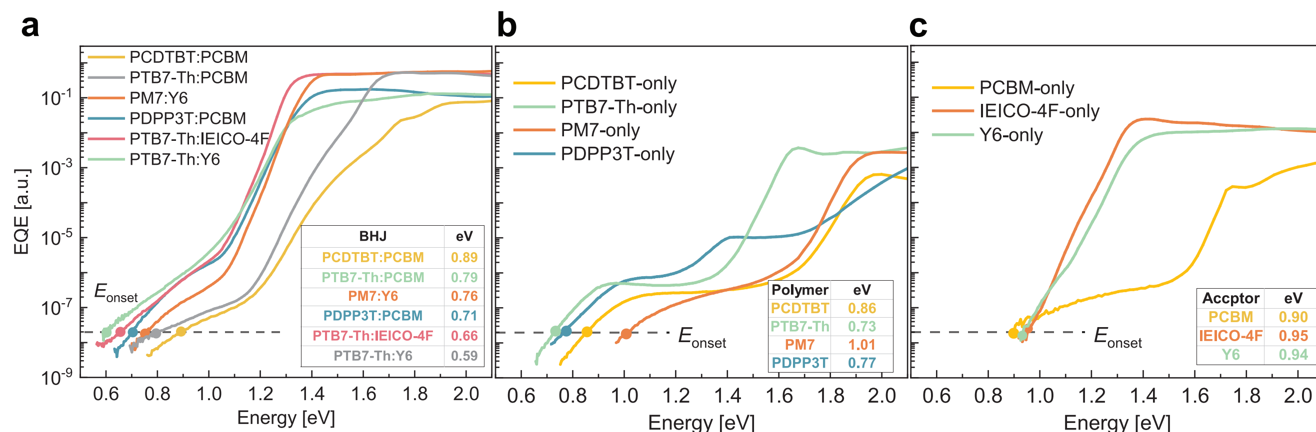

Figure 4. EQE spectra. a) For BHJ layers. b) For donor-only layers. c) For acceptor-only layers. Spectra shown in panel a) were recorded for semi-transparent devices and in panels b,c) for non-transparent devices. All spectra share the same vertical axis.

Supporting Information). Figure 4a further shows that for the six BHJs the order by which E_{onset} (somewhat arbitrarily defined at EQE = 2×10^{-8}) increases, correlates with the order of increasing E_a in Table 1. More specifically, E_{onset} is between 0.59 (for PTB7-Th:Y6) and 0.89 eV (for PCDTBT:PCBM) and thus in the same range as E_a (0.54 – 0.86 eV, Table 1). The correspondence between E_a and E_{onset} corroborates that thermal and photo-induced charge carrier generation use the same intra-gap states in BHJ layers and have the same minimal energy for charge generation. The energies found in these two completely independent experiments are much less than E_g^{eff} and indicate that charge generation occurs via intra-gap states.

To better identify the origin of these intra-gap states in BHJs, the EQE spectra of donor-only and acceptor-only devices were recorded. All donor-only diodes show a distinct sub-bandgap feature below the exponential band edge similar to the BHJs, and their low-energy onsets range from 0.73 eV (for PTB7-Th) to 1.01 eV (for PM7). These onsets do not scale proportional to the optical bandgaps of the donors, thereby suggesting that the shape of the density of states (DOS) at the band edges varies considerably among the different donors. For the acceptor-only spectra, the non-fullerene acceptors (NFAs) Y6 and IEICO-4F show no clear evidence of sub-bandgap transitions below their exponential band edges, while for the fullerene acceptor PCBM a broad sub-bandgap EQE signal appears. Thus, the low-energy signals observed in the EQE spectra of BHJs comprising either Y6 or IEICO-4F (Figure 4a) likely originate from intra-gap states in the donor phase.

3. Conclusion

In this work, we have identified the origin of reverse dark current (J_d) in optimized organic BHJ photodiodes. By measuring J_d as function of temperature and of donor-acceptor ratio, we show that J_d is dominated by thermal generation of charge carriers via intra-gap states in the BHJ. The existence of the intra-gap states is confirmed by the appearance of low-energy signals in sub-bandgap photocurrent spectra. The close correspondence of the thermal activation energy of the reverse dark current, E_a, and the low-energy onset of photocurrent, E_{onset}, indicates that the lowest energies for thermal and optical charge generation are the same in these blends. Surprisingly, E_a and E_{onset} are also similar to qV_{OC}, the energy that measures the quasi-Fermi levels for holes and electrons in the DOS under illumination. **Figure 5** shows a schematic band diagram and DOS for the BHJs that emerges from these results. The intra-gap states involved in dark current generation correspond to the dark areas in Figure 5 positioned within the effective bandgap. The arrow indicates how thermal and optical charge generation share the same excitation energies. As suggested by the sub-bandgap EQE spectra of donor- and acceptor-only diodes (Figure 4b,c), the density of intra-gap states differs considerably among the materials studied and is lowest for the two NFAs.

Because thermal charge generation via intra-gap states has been identified as the main origin of J_d in optimized OPD configurations, a further reduction of J_d requires reducing the density of intra-gap states or moving their energies closer to the band edges by improved molecular engineering of organic semiconductor materials. Because the two NFAs studied appear almost devoid of intra-gap states, improvements in the donor materials seem the most effective approach here. This is particularly crucial for achieving high-performance OPDs

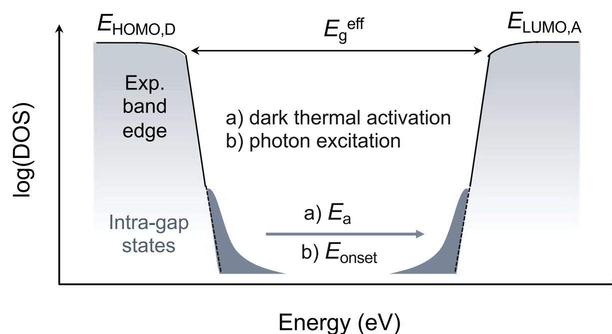

Figure 5. Intra-gap states with energies positioned between the exponential band edges of the HOMO and LUMO are shown as dark gray shadowed areas. The gray single arrow denotes how thermal generation (E_a) and photon excitation (E_{onset}) of charge carriers via intra-gap states can occur. Note that among the acceptors studied, IEICO-4F and Y6 appear almost devoid of intra-gap states compared to PCBM (Figure 4c).

 © 2022 The Authors. Advanced Materials published by Wiley-VCH GmbH

that operate in the near-infrared, where the effective bandgap is intrinsically small.

4. Experimental Section

Materials and Device Fabrication: Details of materials and device fabrication are provided in the Supporting Information.

Device Characterization: The UPS measurements were performed with the VG EscaLab II system under a base pressure of 10^{-8} Pa. The He–I radiation of 21.22 eV and a bias of −6 V were used during measurement. Temperature dependent *J–V* characteristics were measured in a cryostat under vacuum (10^{-4} mbar) and temperature was controlled by a Lake Shore 336 temperature controller. A LabView code was used to program temperature and source meter (Keithley 2636A). *J–V* characteristics were measured with voltage steps of 1 mV. Current density at different temperatures was recorded under a certain voltage bias for 5 min and an average value of the last minute was defined as the current density. The setup for sub-bandgap EQE spectroscopy measurement consisted of a tungsten-halogen lamp (250 W), a chopper (Oriel 3502), a monochromator (Oriel, Cornerstone 260), a preamplifier (Stanford Research Systems SR570), and a lock-in amplifier (Stanford Research SR830). A series of long pass filters with increasing cut-on wavelengths was placed between the lamp and monochromator to remove stray light during the measurement. The monochromatic light is then passed through a concave cylindrical lens, to focus the light and increase the intensity on the active area of the device. Reference Si and InGaAs photodiodes were used to calibrate the incident light intensity. The noise measurement setup is integrated in a metal enclosure to shield from electromagnetic interference. A battery-powered current to voltage conversion readout circuit is developed with off-the-shelf components. The diodes were connected to a trans-impedance amplifier (TIA) implemented with an operational amplifier (Analog Devices ADA4530). An adjustable DC voltage source was applied to the non-inverting terminal of the TIA to modify the bias of device. The output of the TIA was fed to an active bandpass amplifier (implemented with the Analog Devices AD8065) and read out by a dynamic signal analyzer (HP35670A).

Supporting Information

Supporting Information is available from the Wiley Online Library or from the author.

Acknowledgements

The authors thank the process engineers of Holst Centre's R&D Pilot Line for the fabrication of the OPD substrates. The authors acknowledge funding from the Ministry of Education, Culture, and Science (Gravity program 024.001.035) and from Netherlands Organisation for Scientific Research (NWO Spinoza grant). The work is further part of the Advanced Research Center for Chemical Building Blocks, ARC CBBC, which is co-founded and co-financed by Netherlands Organisation for Scientific Research (NWO) and the Netherlands Ministry of Economic Affairs (project 2016.03.Tue).

Conflict of Interest

The authors declare no conflict of interest.

Author Contributions

X.M. fabricated and characterized the devices. H.B. synthesized PM7. B.T.v.G. performed sensitive EQE measurements. X.M., B.T.v.G., and T.P.A.v.d.P. analyzed the EQE spectra. M.J.D. wrote the LabView code for temperature dependent *J–V* characteristics. C.H.L.W. performed UPS experiments. M.F. developed the noise setup. D.T. and A.J.J.M.v.B. optimized the processes of OPD substrates. X.M., S.C.J.M., R.A.J.J., and G.H.G. planned the research and interpreted the data. X.M. wrote the manuscript with help of R.A.J.J. and G.H.G. All authors commented on it.

Data Availability Statement

The data that support the findings of this study are available from the corresponding author upon reasonable request.

Keywords

bulk-heterojunction, dark current, organic photodiodes, organic semiconductors

Received: October 18, 2022
Revised: November 21, 2022
Published online: December 21, 2022

[1] H. Xu, J. Liu, J. Zhang, G. Zhou, N. Luo, N. Zhao, *Adv. Mater.* **2017**, *29*, 1700975.
[2] C. M. Lochner, Y. Khan, A. Pierre, A. C. Arias, *Nat. Commun.* **2014**, *5*, 5745.
[3] Z. Wu, Y. Zhai, W. Yao, N. Eedugurala, S. Zhang, L. Huang, X. Gu, J. D. Azoulay, T. N. Ng, *Adv. Funct. Mater.* **2018**, *28*, 1805738.
[4] G. H. Gelinck, A. Kumar, J.-L. van der Steen, U. Shafique, P. E. Malinowski, K. Myny, B. P. Rand, M. Simon, W. Rütten, A. Douglas, J. Jorritsma, P. Heremans, R. Andriessen, *Org. Electron.* **2013**, *14*, 2602.
[5] L. Basirico, A. Ciavatti, T. Cramer, P. Cosseddu, A. Bonfiglio, B. Fraboni, *Nat. Commun.* **2016**, *7*, 13063.
[6] S. Yoon, K. M. Sim, D. S. Chung, *J. Mater. Chem. C* **2018**, *6*, 13084.
[7] R. D. Jansen-van Vuuren, A. Armin, A. K. Pandey, P. L. Burn, P. Meredith, *Adv. Mater.* **2016**, *28*, 4766.
[8] D. Tordera, B. Peeters, H. B. Akkerman, A. J. J. M. van Breemen, J. Maas, S. Shanmugam, A. J. Kronemeijer, G. H. Gelinck, *Adv. Mater. Technol.* **2019**, *4*, 1900651.
[9] L. Perdigón-Toro, H. Zhang, A. Markina, J. Yuan, S. M. Hosseini, C. M. Wolff, G. Zuo, M. Stolterfoht, Y. Zou, F. Gao, D. Andrienko, S. Shoaee, D. Neher, *Adv. Mater.* **2020**, *32*, 1906763.
[10] M. Liu, Q. Fan, J. Wang, F. Lin, Z. Zhao, K. Yang, X. Zhao, Z. Zhou, A. K.-Y. Jen, F. Zhang, *ACS Appl. Mater. Interfaces* **2022**, *14*, 45636.
[11] M. Hiramoto, T. Imahigashi, M. Yokoyama, *Appl. Phys. Lett.* **1994**, *64*, 187.
[12] Z. Zhao, B. Liu, C. Xu, L. Li, M. Liu, K. Yang, S. Y. Jeong, H. Y. Woo, G. Yuan, W. Li, F. Zhang, *J. Mater. Chem. C* **2022**, *10*, 7822.
[13] J. Kublitski, A. Fischer, S. Xing, L. Baisinger, E. Bittrich, D. Spoltore, J. Benduhn, K. Vandewal, K. Leo, *Nat. Commun.* **2021**, *12*, 4259.
[14] Z. Zhao, C. Xu, Y. Ma, K. Yang, M. Liu, X. Zhu, Z. Zhou, L. Shen, G. Yuan, F. Zhang, *Adv. Funct. Mater.* **2022**, *32*, 2203606.
[15] A. Pierre, I. Deckman, P. B. Lechêne, A. C. Arias, *Adv. Mater.* **2015**, *27*, 6411.
[16] J. B. Park, J.-W. Ha, S. C. Yoon, C. Lee, I. H. Jung, D.-H. Hwang, *ACS Appl. Mater. Interfaces* **2018**, *10*, 38294.
[17] S. Wu, B. Xiao, B. Zhao, Z. He, H. Wu, Y. Cao, *Small* **2016**, *12*, 3374.
[18] X. Gong, M.-H. Tong, S. H. Park, M. Liu, A. Jen, A. J. Heeger, *Sensors* **2010**, *10*, 6488.
[19] S. Valouch, C. Hönes, S. W. Kettlitz, N. Christ, H. Do, M. F. G. Klein, H. Kalt, A. Colsmann, U. Lemmer, *Org. Electron.* **2012**, *13*, 2727.

© 2022 The Authors. Advanced Materials published by Wiley-VCH GmbH

15214095, 2023, 8, Downloaded from https://onlinelibrary.wiley.com/doi/10.1002/adma.202209598 by Technical University Eindhoven, Wiley Online Library on [03/03/2023]. See the Terms and Conditions (https://onlinelibrary.wiley.com/terms-and-conditions) on Wiley Online Library for rules of use; OA articles are governed by the applicable Creative Commons License

[20] S. Xiong, L. Li, F. Qin, L. Mao, B. Luo, Y. Jiang, Z. Li, J. Huang, Y. Zhou, *ACS Appl. Mater. Interfaces* **2017**, *9*, 9176.
[21] X. Wang, J. Huang, J. Li, J. Yu, *J. Phys. D: Appl. Phys.* **2016**, *49*, 075102.
[22] C.-C. Lee, S. Biring, S.-J. Ren, Y.-Z. Li, M.-Z. Li, N. R. Al Amin, S.-W. Liu, *Org. Electron.* **2019**, *65*, 150.
[23] W. Yang, W. Qiu, E. Georgitzikis, E. Simoen, J. Serron, J. Lee, I. Lieberman, D. Cheyns, P. Malinowski, J. Genoe, H. Chen, P. Heremans, *ACS Appl. Mater. Interfaces* **2021**, *13*, 16766.
[24] M. Kielar, O. Dhez, G. Pecastaings, A. Curutchet, L. Hirsch, *Sci. Rep.* **2016**, *6*, 39201.
[25] E. Saracco, B. Bouthinon, J. M. Verilhac, C. Celle, N. Chevalier, D. Mariolle, O. Dhez, J. P. Simonato, *Adv. Mater.* **2013**, *25*, 6534.
[26] H. Shekhar, O. Solomeshch, D. Liraz, N. Tessler, *Appl. Phys. Lett.* **2017**, *111*, 223301.
[27] J. Kublitski, A. Hofacker, B. K. Boroujeni, J. Benduhn, V. C. Nikolis, C. Kaiser, D. Spoltore, H. Kleemann, A. Fischer, F. Ellinger, K. Vandewal, K. Leo, *Nat. Commun.* **2021**, *12*, 551.
[28] N. Zarrabi, O. J. Sandberg, S. Zeiske, W. Li, D. B. Riley, P. Meredith, A. Armin, *Nat. Commun.* **2020**, *11*, 5567.
[29] S. Karuthedath, J. Gorenflot, Y. Firdaus, N. Chaturvedi, C. S. P. De Castro, G. T. Harrison, J. I. Khan, A. Markina, A. H. Balawi, T. A. Dela Peña, W. Liu, R.-Z. Liang, A. Sharma, S. H. K. Paleti, W. Zhang, Y. Lin, E. Alarouso, S. Lopatin, D. H. Anjum, P. M. Beaujuge, S. De Wolf, I. McCulloch, T. D. Anthopoulos, D. Baran, D. Andrienko, F. Laquai, *Nat. Mater.* **2021**, *20*, 378.
[30] H. Yoshida, *J. Phys. Chem. C* **2014**, *118*, 24377.
[31] G. Simone, M. J. Dyson, C. H. Weijtens, S. C. Meskers, R. Coehoorn, R. A. Janssen, G. H. Gelinck, *Adv. Opt. Mater.* **2020**, *8*, 1901568.
[32] C. Fuentes-Hernandez, W.-F. Chou, T. M. Khan, L. Diniz, J. Lukens, F. A. Larrain, V. A. Rodriguez-Toro, B. Kippelen, *Science* **2020**, *370*, 698.
[33] S. Gielen, C. Kaiser, F. Verstraeten, J. Kublitski, J. Benduhn, D. Spoltore, P. Verstappen, W. Maes, P. Meredith, A. Armin, K. Vandewal, *Adv. Mater.* **2020**, *32*, 2003818.
[34] X. Zhou, D. Yang, D. Ma, *Adv. Opt. Mater.* **2015**, *3*, 1570.
[35] Y. Song, Z. Zhong, P. He, G. Yu, Q. Xue, L. Lan, F. Huang, *Adv. Mater.* **2022**, *34*, 2201827.
[36] H. J. Eun, H. Lee, Y. Shim, G. U. Seo, A. Y. Lee, J. J. Park, J. Heo, S. Park, J. H. Kim, *iScience* **2022**, *25*, 104194.
[37] W. F. Pasveer, J. Cottaar, C. Tanase, R. Coehoorn, P. A. Bobbert, P. W. M. Blom, D. M. De Leeuw, M. A. J. Michels, *Phys. Rev. Lett.* **2005**, *94*, 206601.
[38] K. Vandewal, K. Tvingstedt, A. Gadisa, O. Inganäs, J. V. Manca, *Nat. Mater.* **2009**, *8*, 904.
[39] K. Tvingstedt, K. Vandewal, A. Gadisa, F. Zhang, J. Manca, O. Inganäs, *J. Am. Chem. Soc.* **2009**, *131*, 11819.
[40] J. Benduhn, K. Tvingstedt, F. Piersimoni, S. Ullbrich, Y. Fan, M. Tropiano, K. A. McGarry, O. Zeika, M. K. Riede, C. J. Douglas, S. Barlow, S. R. Marder, D. Neher, D. Spoltore, K. Vandewal, *Nat. Energy* **2017**, *2*, 17053.
[41] M. C. Scharber, D. Mühlbacher, M. Koppe, P. Denk, C. Waldauf, A. J. Heeger, C. J. Brabec, *Adv. Mater.* **2006**, *18*, 789.
[42] B. T. van Gorkom, T. P. A. van der Pol, K. Datta, M. M. Wienk, R. A. J. Janssen, *Nat. Commun.* **2022**, *13*, 349.
[43] C. Kaiser, S. Zeiske, P. Meredith, A. Armin, *Adv. Opt. Mater.* **2020**, *8*, 1901542.

© 2022 The Authors. Advanced Materials published by Wiley-VCH GmbH

15214095, 2023, 8, Downloaded from https://onlinelibrary.wiley.com/doi/10.1002/adma.202209598 by Technical University Eindhoven, Wiley Online Library on [03/03/2023]. See the Terms and Conditions (https://onlinelibrary.wiley.com/terms-and-conditions) on Wiley Online Library for rules of use; OA articles are governed by the applicable Creative Commons License